Journal of Applied Physics

RESEARCH ARTICLE | APRIL 05 2023

Temperature-dependent thermal conductivity of $Ge_2Sb_2Te_5$ polymorphs from 80 to 500 K

Qinshu Li ; Or Levit ; Eilam Yalon ; Bo Sun

Journal of Applied Physics 133, 135105 (2023)
https://doi.org/10.1063/5.0142536

AIP Publishing

Journal of Applied Physics ARTICLE scitation.org/journal/jap

Temperature-dependent thermal conductivity of $Ge_2Sb_2Te_5$ polymorphs from 80 to 500 K

Cite as: J. Appl. Phys. **133**, 135105 (2023); doi: 10.1063/5.0142536
Submitted: 21 January 2023 · Accepted: 19 March 2023 ·
Published Online: 5 April 2023

Qinshu Li,[1] Or Levit,[2] Eilam Yalon,[2,a)] and Bo Sun[1,3,a)]

AFFILIATIONS

[1]Tsinghua-Berkeley Shenzhen Institute, Tsinghua University, Shenzhen 518055, China
[2]Viterbi Faculty of Electrical and Computer Engineering, Technion-Israel Institute of Technology, Haifa 3200003, Israel
[3]Tsinghua Shenzhen International Graduate School and Guangdong Provincial Key Laboratory of Thermal Management Engineering and Materials, Shenzhen 518055, China

[a)]**Authors to whom correspondence should be addressed:** eilamy@technion.ac.il and sun.bo@sz.tsinghua.edu.cn

ABSTRACT

We report the thermal conductivity of amorphous, cubic, and hexagonal $Ge_2Sb_2Te_5$ using time-domain thermoreflectance from 80 to 500 K. The measured thermal conductivities are 0.20 W m^{-1} K^{-1} for amorphous $Ge_2Sb_2Te_5$, 0.63 W m^{-1} K^{-1} for the cubic phase, and 1.45 W m^{-1} K^{-1} for the hexagonal phase at room temperature. For amorphous $Ge_2Sb_2Te_5$, the thermal conductivity increases monotonically with temperature when $T < 300$ K, showing a typical glass-like temperature dependence, and increases dramatically after heating up to 435 K due to partial crystallization to the cubic phase. For hexagonal $Ge_2Sb_2Te_5$, electronic contribution to thermal conductivity is significant. The lattice thermal conductivity of the hexagonal phase shows a relatively low value of 0.47 W m^{-1} K^{-1} at room temperature and has a temperature dependence of T^{-1} when $T > 100$ K, suggesting that phonon–phonon scattering dominates its lattice thermal conductivity. Although cubic $Ge_2Sb_2Te_5$ has a similar grain size to hexagonal $Ge_2Sb_2Te_5$, its thermal conductivity shows a glass-like trend like that of the amorphous phase, indicating a high concentration of vacancies that strongly scatter heat-carrying phonons. These thermal transport mechanisms of $Ge_2Sb_2Te_5$ polymorphs help improve the thermal design of phase change memory devices for more energy-efficient non-volatile memory.

I. INTRODUCTION

With the rapid development of information technology, the demand for data storage is growing at an exponential rate.[1] To respond to the influx of information, data storage devices with higher capacity, faster operation speed, and lower power consumption are needed. Phase change memory (PCM), a promising family of non-volatile memory, can address these challenges and provide great scalability and stability.[2,3] In PCM cells, a chalcogenide thin film can switch repeatedly and rapidly from their high resistivity amorphous phase to a low resistivity crystalline phase (SET) and vice versa (RESET),[3–5] thus undergo the data write and erase processes.[6]

Since the switching between SET and RESET is typically achieved by joule heating, thermal properties of PCM devices have an important impact on every figure of merit including scalability, reliability, and programming current.[7–9] Therefore, knowledge about thermal properties of phase change materials is of vital importance to optimize the performance of PCM devices.[10,11] For example, the thermal conductivity of phase change chalcogenides affects the voltage and current in SET/RESET transition.[12] At the nanoscale, a decrease in the effective thermal conductivity, introduced by increasing interfacial thermal resistance, presents an opportunity to lower energy consumption through reducing operating current.[11,13–15] Aryana *et al.*[11] have suggested that RESET current can be reduced up to ~50% depending on the device lateral size if the thermal boundary resistance between PCM and tungsten changes from 1 to 100 m^2 K GW^{-1}. Reifenberg *et al.* have shown that introducing a thermal boundary resistance of 50 m^2 K GW^{-1} between GST and the bottom electrode can achieve a reduction of ~20% for 25- and 50-nm-thick GST layers and ~30% for 75- and 100-nm-thick GST layers in programming current, which results from an increased lateral temperature uniformity in GST films.[13] Research has emphasized that a reduction in programming current

and switching power as well as an increase in operation speed through thermal design are the key factors for the successful development of PCM technology.[2,10,12] Enhancing the thermal efficiency of PCM-based applications has motivated research on thermal transport properties of phase change chalcogenides.

Germanium-antimony-tellurium, $Ge_2Sb_2Te_5$ (GST), has been the most ubiquitous phase change material and its thermal properties have gained intensive interest.[16,17] From the reported results, however, large discrepancy remains among the measured thermal conductivities. For example, the reported thermal conductivity falls in a wide range of 0.29–0.95 W m^{-1} K^{-1} for GST with a face-centered cubic (FCC) structure (c-GST)[18–22] and 0.77–2.14 W m^{-1} K^{-1} for GST with a hexagonal close-packed (HCP) structure (h-GST),[20,21,23] which were measured by 3ω method[19,22] and thermoreflectance techniques[21,23] including time-domain thermoreflectance (TDTR).[18,20] Besides, the temperature-dependent thermal conductivity of GST also shows inconsistency, especially for c-GST. Lyeo *et al.*[20] have observed that the thermal conductivity of c-GST increases with temperatures, while other measured values show weak or no temperature dependence.[18,21,24] Moreover, thermal transport mechanisms of GST polymorphs have not been well understood until now. And this knowledge requires thermal conductivity measured below their Debye temperatures, which is still absent in literature. Therefore, further exploration of thermophysical properties of GST is still needed.

In this work, we report thermal conductivity of amorphous, cubic, and hexagonal GST films from 80 to 500 K measured using TDTR. We used multiple modulation frequencies in our measurement to simultaneously determine both thermal conductivity (Λ) and heat capacity (C), as heat capacity are lacking in literature when T < 150 K. This study aims to fill the gap in experimental data of thermal properties as well as to provide information about thermal transport mechanisms of GST polymorphs, which is essential for the improvement in performance of PCM devices.

II. SAMPLE PREPARATION AND MATERIAL ANALYSIS

GST thin films with thickness of ∼200 nm were deposited at room temperature on a Si wafer with a thermally grown ∼100-nm-thick SiO_2 layer using RF sputtering. As deposited, the GST films are amorphous (a-GST). We then annealed one sample at 180 °C to form c-GST and another sample at 400 °C to form h-GST, both for 20 min. An Al thin film was deposited on all samples as a transducer for TDTR measurements. The cross-sectional schematic of the sample structure and measurement is shown in Fig. 1(a). Scanning electron microscope (SEM) was used to characterize the cross-sectional structure and thickness of the GST samples, as shown in Figs. 1(b)–1(d).

To identify the phase of each GST sample, x-ray diffraction (XRD) was performed using Cu K_α radiation (λ = 0.154 18 nm). Figure 2 shows a broad hump for the a-GST sample, indicating its amorphous structure. For thermally annealed samples, a sharp peak at 29.7° indicates the FCC structure for our c-GST sample and a peak at 29° confirms a shift toward the HCP structure for the h-GST sample.[25–27] The average grain size is estimated to be 10–15 nm for both c-GST and h-GST samples using the Scherrer equation with the fullwidth at half maximum from XRD peaks.[28]

III. THERMAL CONDUCTIVITY AND DISCUSSION

We measured the thermal properties of all samples from 80 to 500 K using TDTR, an optical pump-probe technique able to measure thermophysical properties of thin films and bulk materials, such as thermal conductivity,[29,30] thermal conductance,[31] and

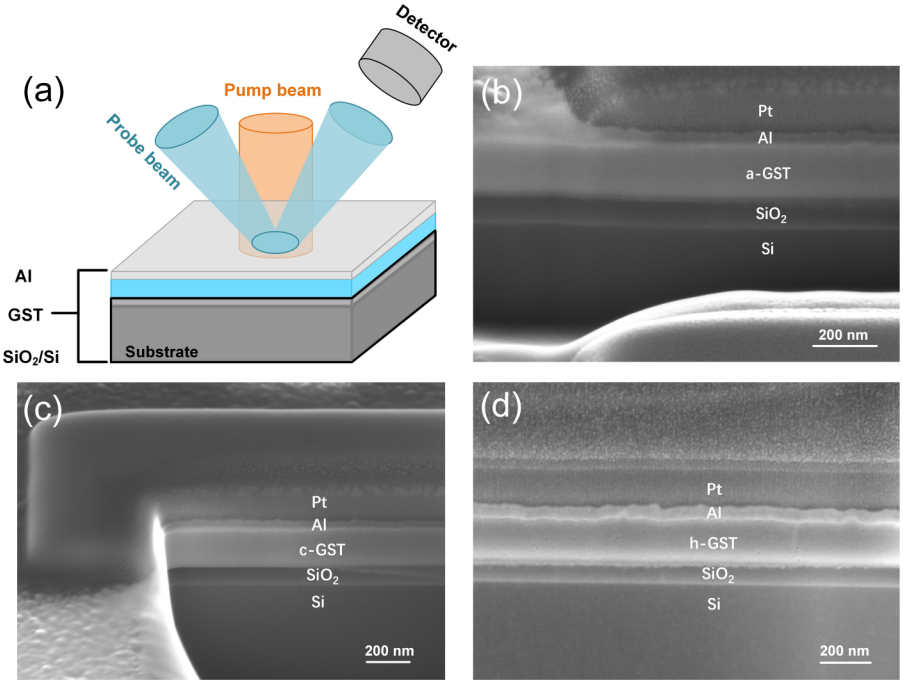

FIG. 1. Structures of GST samples. (a) A schematic of the experimental structure used for TDTR. Cross-sectional SEM images with a scale bar of 200 nm of (b) a-GST, (c) c-GST, and (d) h-GST. Focused ion beam (FIB) was used to prepare samples and Pt layers shown in the SEM images served as a protection layer to protect the surface from incurring FIB-induced damage.

heat capacity.[32] The measurement details and the thermal model have been discussed and can be found in prior reports.[32–34] In our measurement, a $1/e^2$ laser radius of 12 μm was used to ensure heat flow is essentially one-dimensional. When measured above room temperature, a modulation frequency of 10.1 MHz was used, leading the heat flow to penetrate a limited depth into the GST layer. For the low temperature range (80 K < T < 300 K), multiple modulation frequencies were used to obtain both heat capacity (C_{GST}) and thermal conductivity (Λ_{GST}) of GST, as C_{GST} is not available in literature when T < 150 K. For the whole temperature range, the total power used for the pump beam and the probe beam was within 50 mW, introducing a steady-state temperature rise lower than 10 K. The thickness of the Al transducer can be determined accurately by *in situ* picosecond acoustic echoes during the TDTR measurement with an uncertainty of ~3 nm, which is 60.78 nm for a-GST, 57.57 nm for c-GST, and 80.04 nm for h-GST. The thermal conductivity of the Al layer was calculated by Wiedemann–Franz law with the electric resistivity measured by four-point probe, which is 125 W m^{-1} K^{-1} at room temperature. The heat capacity of the Al thin film and GST as well as the thermal properties of the substrate are required in the thermal model and were taken from literature.[35–39]

Before the measurement, we calculated the sensitivities (S_α) of the TDTR signal ($-V_{in}/V_{out}$) to the parameters (α) used in the thermal model[40] as a function of modulation frequency spanning from 0.1 to 20 MHz, which is expressed as follows:

$$S_\alpha = \frac{\partial \ln\left(-\frac{V_{in}}{V_{out}}\right)}{\partial \ln \alpha}. \quad (1)$$

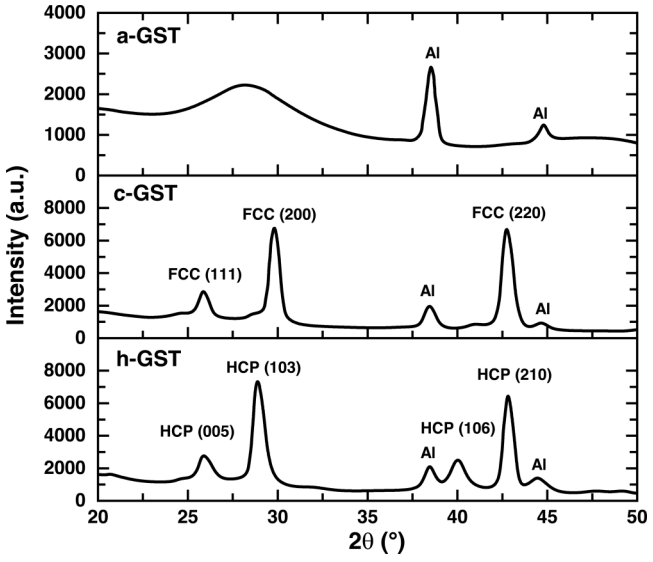

FIG. 2. XRD patterns of the GST samples.

Figure 3(a) shows that the TDTR signal is insensitive to the interface thermal conductance G of Al/a-GST and a-GST/substrate interfaces in this frequency range. The contribution of interface thermal resistance is negligible in our measurement due to large thermal resistivity of a-GST. The TDTR signal is sensitive to the specific heat capacity and thermal conductivity of a-GST, and these sensitivities vary with modulation frequencies. Since the dominant parameters in the thermal response, C_{GST} and Λ_{GST}, are frequency independent, both C_{GST} and Λ_{GST} can be extracted when measured with multiple modulation frequencies.

We measured our 200-nm-thick GST samples at modulation frequencies of 1.01, 4.6, and 10.1 MHz to simultaneously determine Λ_{GST} and C_{GST}, where we fitted the thermal conductivity of GST and the substrate with a fixed C_{GST} value. A demonstration of such measurement at room temperature is shown in Figs. 3(b)–3(e). Under each modulation frequency, the best-fitted Λ_{GST} was determined by minimizing the standard deviation between the model and the experimental dataset [Fig. 3(b)] and varies with C_{GST} [Fig. 3(c)]. We considered an experimental uncertainty (8%) in the Λ-C plot shown in Figs. 3(c)–3(e), which results from the uncertainties of the thickness of Al and GST layers, thermal properties of the Al thin film and substrate, laser spot size, and the phase of the lock-in amplifier. The measured C and Λ of a-GST ($C_{a\text{-}GST}$, $\Lambda_{a\text{-}GST}$) fall in the range of 1.26–1.49 J cm^{-3} K^{-1} and 0.18–0.21 W m^{-1} K^{-1}, where Λ-C curves cross. We chose the center point and determined $C_{a\text{-}GST}$ to be 1.38 ± 0.12 J cm^{-3} K^{-1} and $\Lambda_{a\text{-}GST}$ to be 0.20 ± 0.02 W m^{-1} K^{-1}. We used this method to measure both Λ_{GST} and C_{GST} from 80 to 300 K. The measured Λ_{GST} is shown in Fig. 4 and C_{GST} is shown in Fig. 3(f). We fitted the measured C_{GST} with a proper value of Debye temperature (T_D) using the Debye model.[41] And the T_D for a-GST is determined to be 310 K, which is much higher than the estimated value (136 K) using acoustic properties such as mass density and elastic constants.[42] We argue that the fitted T_D from experiments is more reliable, as optical phonons in complex compounds were not considered properly in estimated T_D.[43] The heat capacities of both h-GST and c-GST can be fitted with the same Debye temperature, 310 K. The measured values of C_{GST} in our measurement suggest that the molar heat capacity of GST polymorphs are similar,[44] and thus, the difference in volumetric heat capacity results from mass densities of GST polymorphs [Fig. 3(f)].

The measured thermal conductivity of GST samples from 80 to 500 K is shown in Fig. 4. At room temperature, the thermal conductivity is 0.20 W m^{-1} K^{-1} for a-GST and increases by a factor of ~3 for c-GST and ~7 for h-GST. Our measured Λ_{GST} at room temperature and above are similar to a few prior measurements, such as by Lyeo *et al.*[20] using TDTR with a 270-nm-thick GST, by Lee *et al.*[45] using TDTR with a 150-nm-thick GST, by Siegert *et al.*[46] using the 3ω method with a 300-nm-thick GST, and by Kuwahara *et al.*[23] using nanosecond thermoreflectance with a 300-nm-thick GST. See Fig. 4(a) for comparison. For a-GST, our values have a difference as large as 45% with the results measured by Reifenberg *et al.*[21] using transient thermoreflectance with a 350-nm-thick GST. For c-GST, the measured results by Reifenberg *et al.*[18] with a 91.4-nm-thick GST also show a weak temperature dependence but with a lower value than this work, which could be due to the contribution of additional thermal resistance from across the top TiN layer and GST interface in

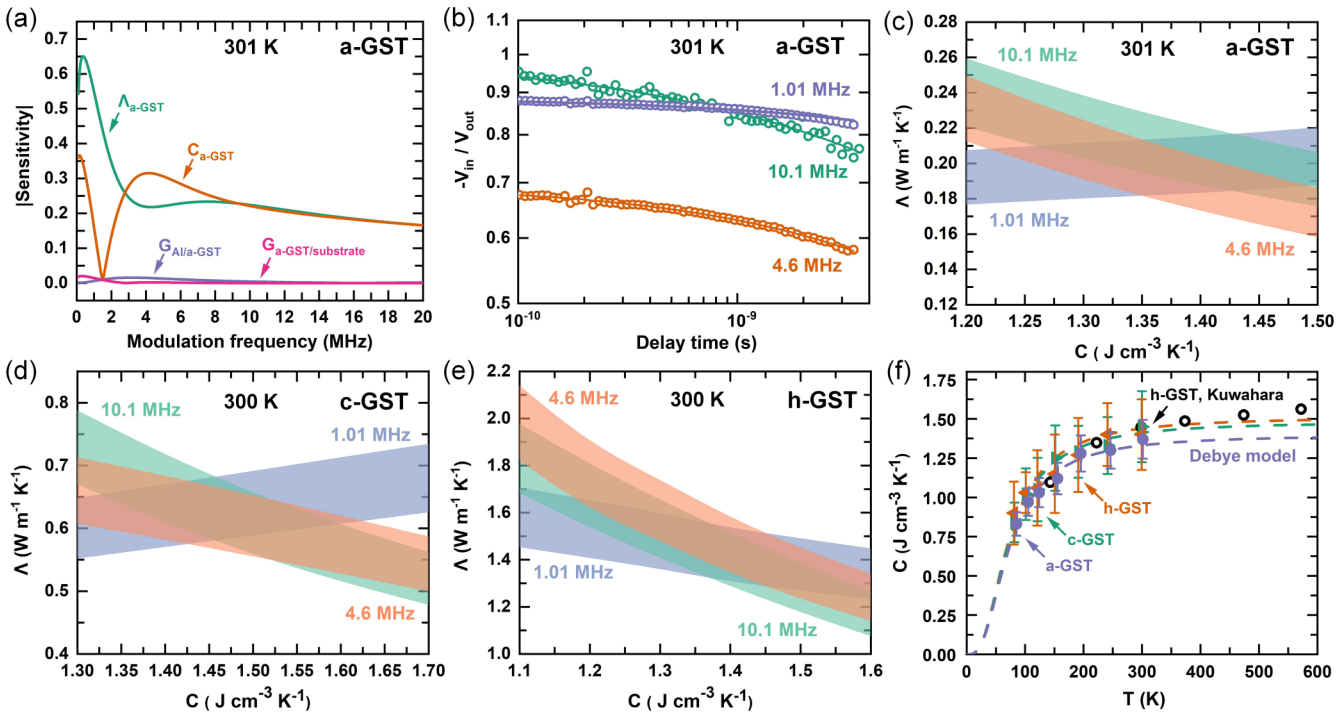

FIG. 3. A demonstration of simultaneous measurement thermal conductivity and heat capacity of GST. (a) The sensitivity of $-V_{in}/V_{out}$ signal to $\Lambda_{a\text{-GST}}$ (green line), $C_{a\text{-GST}}$ (orange line), thermal conductance G of Al/a-GST ($G_{Al/a\text{-GST}}$, purple line), and a-GST/substrate ($G_{a\text{-GST/substrate}}$, pink line) interfaces from 0.1 to 20 MHz at 1 ns delay time. (b) The experimental data (spheres) and best-fit results (lines) for a-GST under 1.01 MHz (purple), 4.6 MHz (orange), and 10.1 MHz (green). The Λ-C plot of (c) a-GST at 301 K, (d) c-GST at 300 K, and (e) h-GST at 300 K, with an experiment uncertainty of 8% considered. (f) The heat capacity obtained from the TDTR measurement (purple spheres for a-GST, green right triangles for c-GST, and orange left triangles for h-GST), C of h-GST from literature[23] (open spheres) and fitted using the Debye model[41] with a Debye temperature of 310 K (dashed lines).

their measurement. And the c-GST measured by Kuwahara *et al.*[24] using nanosecond thermoreflectance shows no obvious temperature dependence, probably resulting from suppressed crystallization in their 60-nm-thick GST thin film due to the increasing stress from the interfaces.[47]

As shown in Fig. 4(a), $\Lambda_{a\text{-GST}}$ increases slightly with temperatures from 80 to 200 K, above which it remains constant until phase transition at 435 K, where the thermal conductivity increases dramatically. The measured thermal conductivity at 435 K is 0.50 W m^{-1} K^{-1} after the GST film partially crystalized. This value is 26% lower than that of c-GST (0.68 W m^{-1} K^{-1} at 435 K), which was annealed for 20 min at 453 K, suggesting that the a-GST film heated to 435 K during the TDTR measurement underwent partial crystallization.[25,46] A lower limit for the thermal conductivity of a-GST (Λ_{min}) can be calculated by the Cahill–Pohl model,[48] assuming random walk of energy between neighboring oscillators to describe thermal transport. Here, we used the Debye temperature $T_D = 310$ K, which was extracted from our heat capacity measurements in Fig. 3(f). Our measured $\Lambda_{a\text{-GST}}$ shows the same temperature dependence as Λ_{min} [Fig. 4(a)], demonstrating a typical amorphous-like transport behavior. As lattice vibrations in the model are based on the Debye model, the predictions show imperfect quantitative agreement with experiment results.[48]

Of all three phases, h-GST has the highest thermal conductivity throughout the measured temperature range from 80 to 500 K, as shown in Fig. 4(a). At room temperature, it has a thermal conductivity of 1.45 W m^{-1} K^{-1}. Unlike a-GST and c-GST, the electronic contribution to thermal conductivity (Λ_e) is non-negligible in h-GST.[16,49,50] To investigate its phonon transport behavior, Λ_e was subtracted from the measured total thermal conductivity (Λ_{tot}), which was calculated based on the Wiedemann–Franz law and the electrical resistivity.[49] At room temperature, the lattice thermal conductivity (Λ_{ph}) is 0.47 W m^{-1} K^{-1} and Λ_e contributes 68% of the Λ_{tot} [Fig. 4(b)], which is similar to prior results of the h-GST thin film.[20,45] Lyeo *et al.*[20] have reported that Λ_{ph} is 0.48 W m^{-1} K^{-1} and Λ_e contributes nearly 70% of Λ_{tol}. The values measured by Lee *et al.*[45] also show that Λ_{ph} is 0.42 W m^{-1} K^{-1} and Λ_e accounts for 66% of Λ_{tot}. When $T > 100$ K, Λ_{ph} decreases inversely proportional to temperatures, suggesting phonon–phonon scattering dominates its lattice thermal conductivity.[51] Such temperature dependence indicates that h-GST has the high degree of crystallinity and the boundary scattering of phonons is not important with a grain size of 10–15 nm, which is in good agreement with the first-principles calculation that phonons with the mean free path less than 10 nm dominate the lattice thermal conductivity of h-GST.[52]

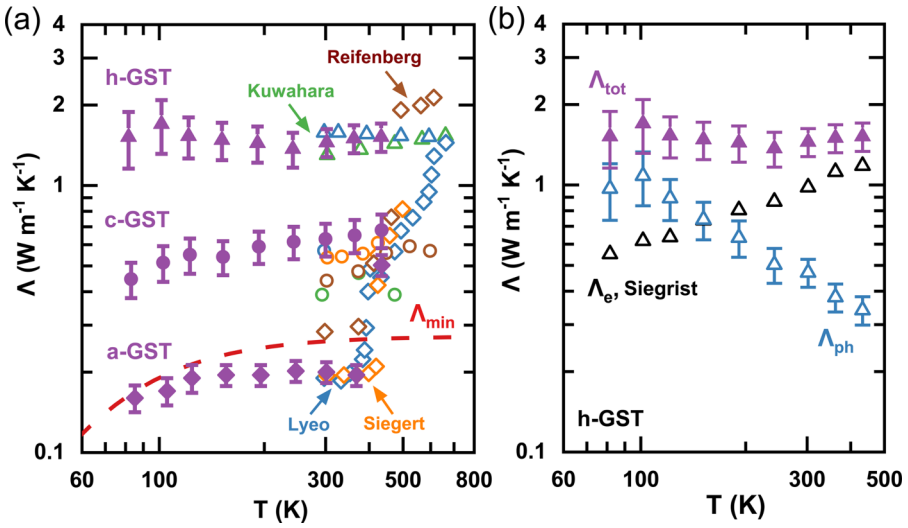

FIG. 4. Thermal conductivity of GST samples from 80 to 500 K. (a) Measured thermal conductivity of a-GST (purple diamonds), c-GST (purple spheres), and h-GST (purple triangles). The lower limit for $\Lambda_{a\text{-}GST}$ (Λ_{min}, red dashed line) is calculated using the Cahill–Pohl model.[48] For comparison, we show prior results of GST polymorphs measured by Lyeo *et al.*[20] (blue diamonds for a-GST along annealed temperatures, blue spheres for c-GST, and blue triangles for h-GST), by Siegert *et al.*[46] (orange diamonds for a-GST and orange spheres for c-GST), by Kuwahara *et al.*[23,24] (green spheres for c-GST and green triangles for h-GST), and by Reifenberg *et al.*[18,21] (brown diamonds for a-GST and brown spheres for c-GST). (b) Measured total (Λ_{tot}, purple triangles) and lattice thermal conductivity (Λ_{ph}, blue triangles) of h-GST. The electronic thermal conductivity (Λ_e) shown in black triangles is calculated using Wiedemann–Franz law and the electrical resistivity.[49]

According to Fig. 2, c-GST has a similar grain size to h-GST; however, its lattice thermal conductivity is in striking contrast to that of h-GST and shows a glass-like trend as that of a-GST [Fig. 4(a)]. This result suggests, besides grain boundary scattering, other phonon scattering process will dominate phonon transport in c-GST. A number of studies have shown that unlike h-GST, c-GST is metastable and has a rock-salt-like structure with Te atoms occupying the anion sites and Ge/Sb plus as much as 20% vacancies randomly occupying the cation sites.[53,54] These intrinsic defects existing in c-GST, including point defects and disordered structures,[55–57] could increase phonon scattering and lead to glass-like thermal conductivity.[20,46] For GST, the transition from an insulating phase to a metallic phase is attributed to the decrease in randomness by ordering vacancies.[50,58] Therefore, adjustment of the concentration and rearrangement of vacancies such as annealing and increasing extrinsic defects could tune the thermal properties of c-GST.[50,59]

IV. CONCLUSIONS

In summary, we measured the thermal conductivity of GST thin films in the temperature range from 80 to 500 K. The thermal conductivity of amorphous GST measured at room temperature is 0.20 W m^{-1} K^{-1} and increases to 0.63 W m^{-1} K^{-1} for cubic GST and 1.45 W m^{-1} K^{-1} for hexagonal GST. In the low temperature range of 80 K < T < 300 K, the thermal conductivity of a-GST increases monotonically with temperatures, showing a typically amorphous-like transport behavior, and then increases close to that of c-GST at 435 K due to partial crystallization. The lattice thermal conductivity of the hexagonal GST shows a relatively low value of 0.47 W m^{-1} K^{-1} at room temperature and decreases with temperatures when T > 100 K, indicating that the phonon–phonon scattering dominates its lattice thermal conductivity though with a small grain size of 10–15 nm. The measured temperature-dependent thermal conductivity of c-GST shows a glass-like trend although it is crystalline, suggesting a large concentration of defects in this metastable phase. Our results can help better understand the thermal transport mechanisms of GST in its different phases, which is important for further development of energy-efficient phase change chalcogenides for non-volatile memory and neuromorphic applications. Future studies should focus on thermal properties at the high temperature range, because during memory switching, these devices will reach their melting temperature (~900 K).

ACKNOWLEDGMENTS

We acknowledge funding support from ISF-NSFC Joint Scientific Research Program (ISF No. 3582/21, NSFC No. 52161145502). B.S. would also like to thank funding support from NSFC (No. 12004211), the Shenzhen Science and Technology Program (Nos. RCYX20200714114643187 and WDZC20200821100123001), and Tsinghua Shenzhen International Graduate School (No. QD2021008N). This work was also supported in part by the Russel Berrie Nanotechnology Institute (RBNI), Technion. Fabrication was carried out at the Technion Micro-Nano Fabrication and Printing Unit (MNF&PU). We thank Guy Ankonina (Technion) for sputtering, Larissa Popilevsky (Technion) for support with focused ion beam cross section microscopy, and Maria Koifman from the Technion Materials

Science and Engineering XRD lab for support with XRD measurements.

AUTHOR DECLARATIONS

Conflict of Interest

The authors have no conflicts to disclose.

Author Contributions

Qinshu Li: Formal analysis (lead); Investigation (lead); Writing – original draft (lead). **Or Levit:** Formal analysis (equal); Methodology (equal). **Eilam Yalon:** Supervision (equal); Writing – original draft (equal). **Bo Sun:** Project administration (equal); Supervision (equal); Writing – original draft (equal).

DATA AVAILABILITY

The data that support the findings of this study are available from the corresponding author upon reasonable request.

REFERENCES

[1]W. Zhang, R. Mazzarello, M. Wuttig, and E. Ma, Nat. Rev. Mater. **4**, 150 (2019).
[2]M. Wuttig, Nat. Mater. **4**, 265 (2005).
[3]P. Guo, A. M. Sarangan, and I. Agha, Appl. Sci. **9**, 530 (2019).
[4]F. Xiong, E. Yalon, A. Behnam, C. M. Neumann, K. L. Grosse, S. Deshmukh, and E. Pop, *2016 IEEE International Electron Devices Meeting* (IEEE, 2016), pp. 4.1.1–4.1.4.
[5]K. Stern, N. Wainstein, Y. Keller, C. M. Neumann, E. Pop, S. Kvatinsky, and E. Yalon, Adv. Electron. Mater. **7**, 2100217 (2021).
[6]S. R. Ovshinsky, Phys. Rev. Lett. **21**, 1450 (1968).
[7]D. Loke, T. H. Lee, W. J. Wang, L. P. Shi, R. Zhao, Y. C. Yeo, T. C. Chong, and S. R. Elliott, Science **336**, 1566, (2012).
[8]G. Bruns, P. Merkelbach, C. Schlockermann, M. Salinga, M. Wuttig, T. D. Happ, J. B. Philipp, and M. Kund, Appl. Phys. Lett. **95**, 043108 (2009).
[9]F. Rao, K. Ding, Y. Zhou, Y. Zheng, M. Xia, S. Lv, Z. Song, S. Feng, I. Ronneberger, R. Mazzarello, W. Zhang, and E. Ma, Science **358**, 1423 (2017).
[10]S. W. Fong, C. M. Neumann, and H. S. P. Wong, IEEE Trans. Electron Devices **64**, 4374 (2017).
[11]K. Aryana, J. T. Gaskins, J. Nag, D. A. Stewart, Z. Bai, S. Mukhopadhyay, J. C. Read, D. H. Olson, E. R. Hoglund, J. M. Howe, A. Giri, M. K. Grobis, and P. E. Hopkins, Nat. Commun. **12**, 774 (2021).
[12]H. S. P. Wong, S. Raoux, S. Kim, J. Liang, J. P. Reifenberg, B. Rajendran, M. Asheghi, and K. E. Goodson, Proc. IEEE **98**, 2201 (2010).
[13]J. P. Reifenberg, D. L. Kencke, and K. E. Goodson, IEEE Electron Device Lett. **29**, 1112 (2008).
[14]G. T. Jeong, Y. N. Hwang, S. H. Lee, S. Y. Lee, K. C. Ryoo, J. H. Park, Y. J. Song, S. J. Ahn, C. W. Jeong, Y. T. Kim, H. Horii, Y. H. Ha, G. H. Koh, H. S. Jeong, and K. Kim, in *2005 International Conference on Integrated Circuit Design and Technology* (IEEE, 2005), pp. 19–22.
[15]C. Ahn, S. W. Fong, Y. Kim, S. Lee, A. Sood, C. M. Neumann, M. Asheghi, K. E. Goodson, E. Pop, and H. S. P. Wong, Nano Lett. **15**, 6809 (2015).
[16]S. Deshmukh, E. Yalon, F. Lian, K. E. Schauble, F. Xiong, I. V. Karpov, and E. Pop, IEEE Trans. Electron Devices **66**, 3816 (2019).
[17]E. Yalon, S. Deshmukh, M. Muñoz Rojo, F. Lian, C. M. Neumann, F. Xiong, and E. Pop, Sci. Rep. **7**, 15360 (2017).
[18]J. P. Reifenberg, K. W. Chang, M. A. Panzer, S. Kim, J. A. Rowlette, M. Asheghi, H. S. P. Wong, and K. E. Goodson, IEEE Electron Device Lett. **31**, 56 (2010).
[19]E. K. Kim, S. I. Kwun, S. M. Lee, H. Seo, and J. G. Yoon, Appl. Phys. Lett. **76**, 3864 (2000).
[20]H. K. Lyeo, D. G. Cahill, B. S. Lee, J. R. Abelson, M. H. Kwon, K. B. Kim, S. G. Bishop, and B. Cheong, Appl. Phys. Lett. **89**, 151904 (2006).
[21]J. P. Reifenberg, M. A. Panzer, S. B. Kim, A. M. Gibby, Y. Zhang, S. Wong, H. S. P. Wong, E. Pop, and K. E. Goodson, Appl. Phys. Lett. **91**, 111904 (2007).
[22]V. Giraud, J. Cluzel, V. Sousa, A. Jacquot, A. Dauscher, B. Lenoir, H. Scherrer, and S. Romer, J. Appl. Phys. **98**, 013520 (2005).
[23]M. Kuwahara, O. Suzuki, Y. Yamakawa, N. Taketoshi, T. Yagi, P. Fons, T. Fukaya, J. Tominaga, and T. Baba, Jpn. J. Appl. Phys. **46**, 3909 (2007).
[24]M. Kuwahara, O. Suzuki, N. Taketoshi, Y. Yamakawa, T. Yagi, P. Fons, K. Tsutsumi, M. Suzuki, T. Fukaya, J. Tominaga, and T. Baba, Jpn. J. Appl. Phys. **45**, 1419 (2006).
[25]J. Lee, T. Kodama, Y. Won, M. Asheghi, and K. E. Goodson, J. Appl. Phys. **112**, 014902 (2012).
[26]F. Fillot and C. Sabbione, J. Appl. Phys. **128**, 235107 (2020).
[27]Z. Xu, C. Chen, Z. Wang, K. Wu, H. Chong, and H. Ye, RSC Adv. **8**, 21040 (2018).
[28]J. I. Langford and A. J. C. Wilson, J. Appl. Crystallogr. **11**, 102 (1978).
[29]B. Sun, G. Haunschild, C. Polanco, J. Ju, L. Lindsay, G. Koblmüller, and Y. K. Koh, Nat. Mater. **18**, 136 (2019).
[30]B. Sun, S. Niu, R. P. Hermann, J. Moon, N. Shulumba, K. Page, B. Zhao, A. S. Thind, K. Mahalingam, J. Milam-Guerrero, R. Haiges, M. Mecklenburg, B. C. Melot, Y. D. Jho, B. M. Howe, R. Mishra, A. Alatas, B. Winn, M. E. Manley, J. Ravichandran, and A. J. Minnich, Nat. Commun. **11**, 6039 (2020).
[31]Q. Li, F. Liu, S. Hu, H. Song, S. Yang, H. Jiang, T. Wang, Y. K. Koh, C. Zhao, F. Kang, J. Wu, X. Gu, B. Sun, and X. Wang, Nat. Commun. **13**, 4901 (2022).
[32]J. Liu, J. Zhu, M. Tian, X. Gu, A. Schmidt, and R. Yang, Rev. Sci. Instrum. **84**, 034902 (2013).
[33]D. G. Cahill, Rev. Sci. Instrum. **75**, 5119 (2004).
[34]B. Sun and Y. K. Koh, Rev. Sci. Instrum. **87**, 064901 (2016).
[35]D. G. Cahill and T. H. Allen, Appl. Phys. Lett. **65**, 309 (1994).
[36]P. D. Desai, J. Phys. Chem. Ref. Data **15**, 967 (1986).
[37]D. A. Ditmars, C. A. Plint, and R. C. Shukla, Int. J. Thermophys. **6**, 499 (1985).
[38]J. Horbach, W. Kob, and K. Binder, J. Phys. Chem. B **103**, 4104 (1999).
[39]M. Asheghi, K. Kurabayashi, R. Kasnavi, and K. E. Goodson, J. Appl. Phys. **91**, 5079 (2002).
[40]B. C. Gundrum, D. G. Cahill, and R. S. Averback, Phys. Rev. B **72**, 245426 (2005).
[41]P. Debye, Ann. Phys. **344**, 789 (1912).
[42]J. L. Battaglia, V. Schick, C. Rossignol, A. Kusiak, I. Aubert, A. Lamperti, and C. Wiemer, Appl. Phys. Lett. **102**, 181907 (2013).
[43]O. L. Anderson, J. Phys. Chem. Solids **12**, 41 (1959).
[44]R. C. Zeller and R. O. Pohl, Phys. Rev. B **4**, 2029 (1971).
[45]J. Lee, E. Bozorg-Grayeli, S. B. Kim, M. Asheghi, H. S. Philip Wong, and K. E. Goodson, Appl. Phys. Lett. **102**, 191911 (2013).
[46]K. S. Siegert, F. R. L. Lange, E. R. Sittner, H. Volker, C. Schlockermann, T. Siegrist, and M. Wuttig, Rep. Prog. Phys. **78**, 013001 (2015).
[47]R. E. Simpson, M. Krbal, P. Fons, A. V. Kolobov, J. Tominaga, T. Uruga, and H. Tanida, Nano Lett. **10**, 414 (2010).
[48]D. G. Cahill, S. K. Watson, and R. O. Pohl, Phys. Rev. B **46**, 6131 (1992).
[49]T. Siegrist, P. Jost, H. Volker, M. Woda, P. Merkelbach, C. Schlockermann, and M. Wuttig, Nat. Mater. **10**, 202 (2011).
[50]W. Zhang, A. Thiess, P. Zalden, R. Zeller, P. H. Dederichs, J. Y. Raty, M. Wuttig, S. Blügel, and R. Mazzarello, Nat. Mater. **11**, 952 (2012).
[51]C. J. Glassbrenner and G. A. Slack, Phys. Rev. **134**, A1058 (1964).
[52]S. Mukhopadhyay, L. Lindsay, and D. J. Singh, Sci. Rep. **6**, 37076 (2016).
[53]B. Zhang, X. P. Wang, Z. J. Shen, X. B. Li, C. S. Wang, Y. J. Chen, J. X. Li, J. X. Zhang, Z. Zhang, S. B. Zhang, and X. D. Han, Sci. Rep. **6**, 25453 (2016).
[54]M. Upadhyay and S. Murugavel, Mater. Today Proc. **67**, 797 (2022).

[55]A. V. Kolobov, P. Fons, A. I. Frenkel, A. L. Ankudinov, J. Tominaga, and T. Uruga, Nat. Mater. **3**, 703 (2004).
[56]J. J. Wang, Y. Z. Xu, R. Mazzarello, M. Wuttig, and W. Zhang, Materials **10**, 862 (2017).
[57]A. Hirata, T. Ichitsubo, P. F. Guan, T. Fujita, and M. W. Chen, Phys. Rev. Lett. **120**, 205502 (2018).
[58]V. Bragaglia, F. Arciprete, W. Zhang, A. M. Mio, E. Zallo, K. Perumal, A. Giussani, S. Cecchi, J. E. Boschker, H. Riechert, S. Privitera, E. Rimini, R. Mazzarello, and R. Calarco, Sci. Rep. **6**, 23843 (2016).
[59]B. Zhang, W. Zhang, Z. Shen, Y. Chen, J. Li, S. Zhang, Z. Zhang, M. Wuttig, R. Mazzarello, E. Ma, and X. Han, Appl. Phys. Lett. **108**, 191902 (2016).